Inorganic Chemistry

Article

pubs.acs.org/IC

3d Element Complexes of Pentadentate Bipyridine-Pyridine-Based Ligand Scaffolds: Structures and Photocatalytic Activities

Cyril Bachmann, Miguel Guttentag, Bernhard Spingler, and Roger Alberto*

Institute of Inorganic Chemistry, University of Zurich, Winterthurerstrasse 190, 8057 Zurich, Switzerland

Supporting Information

ABSTRACT: The synthesis of the two penta-pyridyl type ligands pyridine-2,6-diylbis(dipyridin-2-ylmethanol) (PPy, **1**) and bis-2,2′′-bipyridine-6-yl(pyridine-2-yl)methanol (aPPy, **2**) is described. Both ligands coordinate rapidly to the 3d element cations Mn^{II}, Fe^{II}, Co^{II}, Ni^{II}, Cu^{II}, and Zn^{II}, thereby yielding complexes of the general composition $[MBr(\mathbf{1})]^+$ and $[MBr(\mathbf{2})]^+$, respectively. Further, the X-ray structures of selected complexes with ligands **1** and **2** are described. They show metal center dependent structural features and complexes with **2** exhibiting distinctly distorted octahedral geometries. Moreover, photocatalytic water reduction with $[Co^{II}Br(PPy)]Br$ (**1c**) and $[Co^{II}Br(aPPy)]Br$ (**2c**) as water reducing catalysts (WRC) was investigated. Both complexes showed catalytic activity in water when in presence of ascorbic acid as sacrificial electron donor and $[Re(py)(bpy)(CO)_3]^+$ (**3**) as photosensitizer (PS). Turnover numbers, TONs (H_2/Co), up to 11 000 were achieved. Complex **2c** was more active than **1c**, whereas none of the other complexes showed any activity.

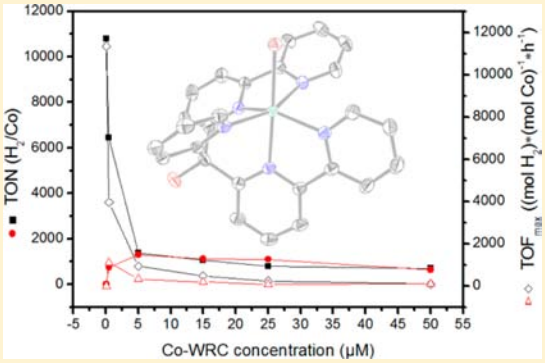

INTRODUCTION

Within a sustainable fuel chain, dihydrogen H_2 forms the basis since it can be converted into liquid fuel by means of well-known industrial processes.[1−3] Hydrogen therefore presents a promising alternative to conventional fossil energy carriers. Nowadays, vast amounts of H_2 are still produced from noncarbon neutral sources such as coal or natural gas. Therefore, the development of efficient and long-term stable systems for splitting water into oxygen and hydrogen by solar light would be an elegant way to unlimited fuel supply.[4−6] Due to the economic relevance and scientific challenge of water splitting, current research efforts focus on both half reactions. For water reduction, catalysts are based on platinum group elements, cobalt,[7−11] iron,[12] nickel,[13] and molybdenum.[14] Cobalt and nickel complexes are among the most active centers in photocatalytic water reduction. Although not directly comparable to the system presented in here, Eisenberg and co-workers recently reported an unprecedented 500 kTON with a dithiolato nickel complex and quantum dots as PS.[15] From the beginning, cobalt complexes with 2,2′-bipyridine (derivatives[16]) and macrocyclic glyoxime as well as tetraimine ligand systems were key players and underwent substantial progress in durability and efficiency ever since.[7,8,17−20] One of the drawbacks for water reducing catalysts with the latter type of ligands is the inherent ligand reducibility, which leads to decomposition of the WRCs and termination of catalysis.[7] Recently, Chang and co-workers introduced polypyridyl ligands similar to **1** and could show high electro- and photocatalytic reactivity with cobalt complexes.[21,22] Zhao and Webster and co-workers achieved remarkable 2100 TON mol H_2 (mol cat)$^{-1}$ with a similar ligand, but comprising a combination of aliphatic and aromatic amines.[23] Our own group recently reported the cobalt-based WRC with a tetra-pyridyl ligand $[Co^{II}Br(TPy)]Br$ (**4**, Scheme 1), which was accomplished with $[Re(py)(bpy)(CO)_3]OTf$ (**3**) as a photosensitizer of about 9000 TON mol H_2 (mol cat)$^{-1}$ in water with $[H_2asc]/[Hasc]^-$ as sacrificial electron donor.[24] The high stability and catalytic activity of polypyridyl cobalt complexes make them superior to cobaloxime complexes.[25] To extend the polypyridyl platform, we synthesized the penta-pyridyl ligand **1**, comprising five individual pyridines as coordinating groups and two hydroxy functions in the backbone. The iron and manganese complexes of **1** have been investigated for hydrogen abstraction reactions, and iron complexes of tetrapodal pentadentate ligands have recently been reviewed by Grohmann et al.[26−28] Cobalt and molybdenum-oxo complexes with derivatives of **1** were studied as WRC in electrocatalytic water reduction.[14,22] As a ligand with the same denticity as **1**, we prepared the less symmetric ligand **2** consisting of two 2,2′-bipyridine units and one single pyridyl donor, preorganized in an arrangement not ideal for pentadentate coordination (Scheme 1). To study structural features and physicochemical properties, 3d element complexes have been synthesized. The cobalt complexes were examined for photocatalytic water reduction in particular.

Received: February 15, 2013
Published: May 3, 2013

   dx.doi.org/10.1021/ic4004017 | Inorg. Chem. 2013, 52, 6055−6061

Scheme 1. Ligand Framework Pentapyridine (PPy, 1) and Alternative Pentapyridine (aPPy, 2) with the Corresponding Metal Complexes (1a–f, 2a–f), Photosensitizer $[Re(py)(bpy)](CO)_3]^+$ (3), and the Previously Used WRC $[Co^{II}Br(TPy)]Br$ (4)[24]

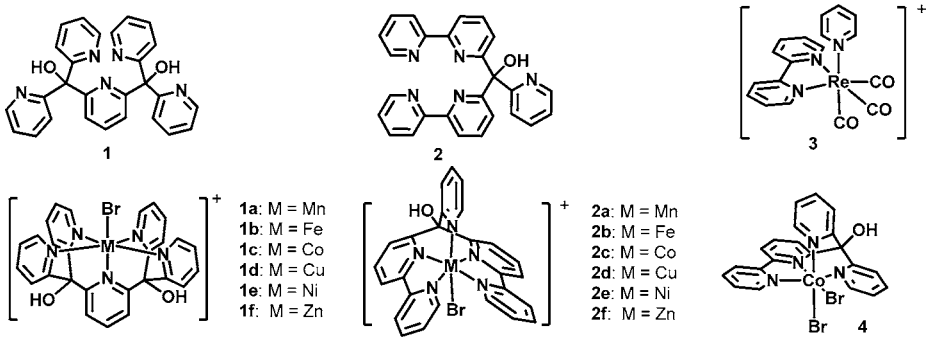

RESULTS AND DISCUSSION

Syntheses and Structures. The new ligand framework **2** (Scheme 1 and Figure 1) was synthesized in two steps: First, nucleophilic addition of lithiated 6-bromo-2,2′-bipyridine (Br-bpy, **5**) to 2-pyridyl ethyl ester gave ketone **6** in yields up to 70%, and a subsequent, second nucleophilic addition of lithiated Br-bpy (**5**) to **6** gave finally the desired ligand **2** in moderate yields of 40–50% (Scheme 2). In the crystal structure of ligand **2** (Figure 1), the single pyridine and the two bipyridine subunits are oriented in a tetrahedral fashion to minimize steric interactions. The two bipyridine units are almost planar, and as it is common for uncoordinated bpy structures, the nitrogen donors point in opposite directions. Whereas ligand **1** offers a coordinating pocket with an almost perfect octahedral arrangement,[26,27] complexes with a tetrapyridyl ligand, such as **4**, display significant distortions from an octahedral geometry.[24] For metal complexes with ligand **2**, we therefore expected very strong deviations from the octahedron and, thus, similar to the entatic principle, differences in reactivity.[29]

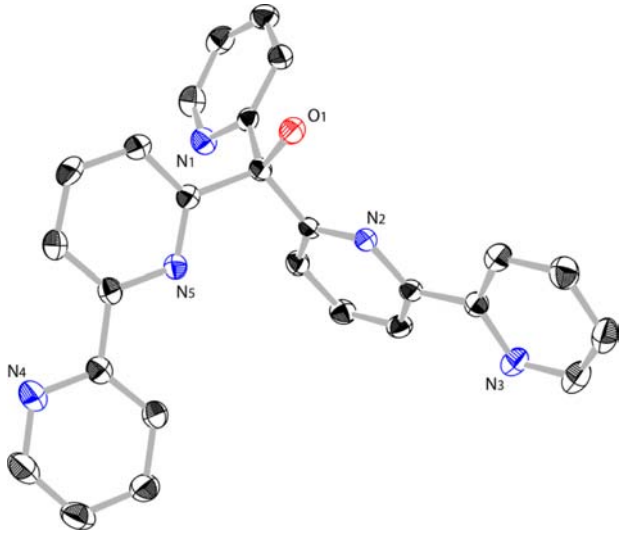

Figure 1. ORTEP drawing of ligand **2** at 50% probability level. Solvent molecules and hydrogen atoms are omitted for clarity.

Scheme 2. Synthetic Strategy for Ligand Framework Alternative Penta-pyridine (aPPy, 2)[a]

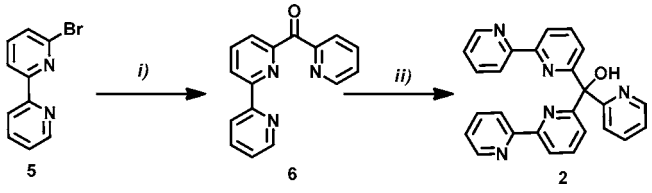

[a](i) nBuLi, 2-ethyl picolinate, −78 to −40 °C, 1 h; (ii) **5**, nBuLi, −78 to −40 °C, 1 h.

Twelve complexes (**1a–f** and **2a–f**) were synthesized by reaction of ligands **1** and **2** with equimolar amounts of MBr_2 (M = Mn, Fe, Co, Ni, Cu, and Zn) in methanol at room temperature. Crystals suitable for single crystal X-ray analysis were obtained by the vapor diffusion method in different solvents (see Experimental Section). Complexes **1a–f** and **2a–f** were characterized by single crystal X-ray crystallography, UV–vis absorption spectroscopy, ESI-MS, and elemental analysis. ^1H NMR measurements were performed for the diamagnetic Zn^{2+} complexes **1f** and **2f**.

The crystal structures of complexes **1a–d** and **1f** (Figure 2 for **1a** (Mn), **1b** (Fe), and **1c** (Co), SI for other structures) show slightly distorted octahedral coordination geometries with four pyridine nitrogen atoms in the equatorial plane, and the disubstituted pyridine nitrogen atom and one bromide in axial positions. An ORTEP representation of complexes **1a–c** is given in Figure 2. Complex **1e** (Cu) gave crystals of low quality (see Supporting Information Figure S24 for picture of the chemical structure), and its structure is thus not further discussed. Stack and co-workers reported a series of related, first row transition metal (Mn–Zn) complexes with a ligand similar to **1**, but with two methoxy instead of two hydroxy groups.[30] The most significant difference for those complexes compared to **1a–f** is the angle between the axial pyridine plane (Py_1 in Figure 2) and the corresponding N_1–M bond (δ_{11}). In complexes with the bis-hydroxy ligand **1**, the pyridine Py_1 is close to perpendicular with respect to the equatorial plane (1.6–6.8° smaller than 90°, Table 1). In the bis-methoxy complexes, this angle is distinctly more bent, probably due to the higher sterical demand of methoxy in comparison with the hydroxy groups. The normal mode of this movement is expected to be of low energy, such that the difference may also be due to the crystal environment.[31] The metal centers in **1a–f** lay slightly above the equatorial plane, and consequently, the angles between N_{ax}–M–N_{eq} (Table 1, α_{11}–α_{14}) are 2.5–9.4° smaller than 90°. Bond angles between the metal center and its axial ligands (γ_{11}) show only small deviations from linearity (by 0.4–4.8°). The highest deviations from octahedral coordination geometry are observed in the equatorial N–M–N angles (β_{11}–β_{14}; −11.5 to +8.5 from 90°, Table 1). ORTEP

dx.doi.org/10.1021/ic4004017 | Inorg. Chem. 2013, 52, 6055–6061

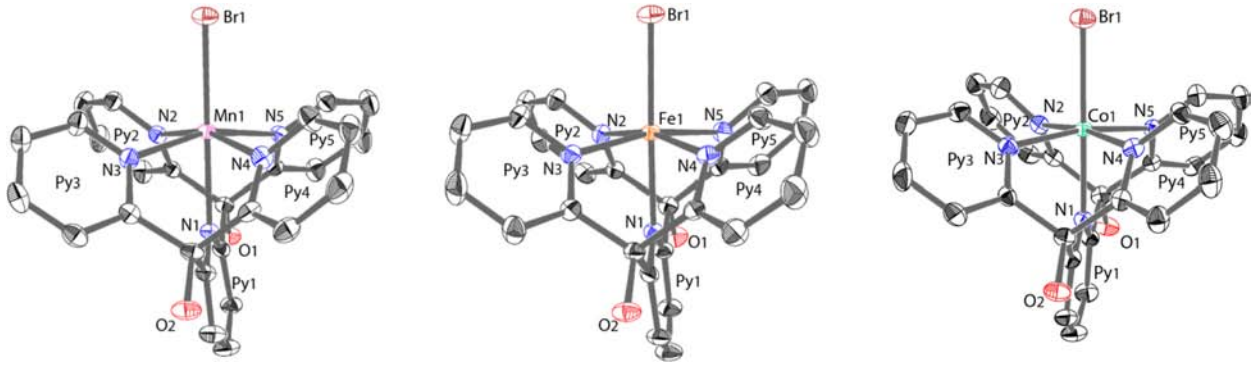

Figure 2. ORTEP drawings of **1a** (left), **1b** (middle), **1c** (right) at 50% probability level with labeled nitrogen atoms and pyridine rings. Counterions, solvent molecules, and hydrogen atoms are omitted for clarity.

Table 1. Selected Bond Angles [deg] of Complexes [MBr(1)]Br

	1a	1b	1c	1d	1f
N_1–M–N_2 (α_{11})	81.75(8)	83.51(9)	86.12(11)	87.5(2)	83.49(12)
N_1–M–N_3 (α_{12})	81.57(9)	83.77(8)	84.90(11)	87.6(2)	82.83(12)
N_1–M–N_4 (α_{13})	82.06(9)	83.48(9)	85.80(11)	86.4(3)	85.27(12)
N_1–M–N_5 (α_{14})	81.67(8)	84.17(8)	85.51(11)	86.4(3)	81.57(12)
N_2–M–N_3 (β_{11})	97.28(9)	97.19(9)	98.47(11)	98.3(3)	96.96(14)
N_3–M–N_4 (β_{12})	79.48(9)	81.03(9)	81.62(11)	82.0519)	79.73(13)
N_4–M–N_5 (β_{13})	98.07(9)	98.56(9)	97.69(11)	96.7(3)	97.27(13)
N_5–M–N_2 (β_{14})	80.40(9)	80.45(9)	80.86(11)	82.28(19)	83.21(14)
N_1–M–Br (γ_{11})	175.24(6)	176.04(6)	176.77(8)	179.6(2)	177.14(8)
Py_1–N_1–M (δ_{11})	173.22(12)	174.30(12)	175.23(16)	177.1(4)	178.37(18)

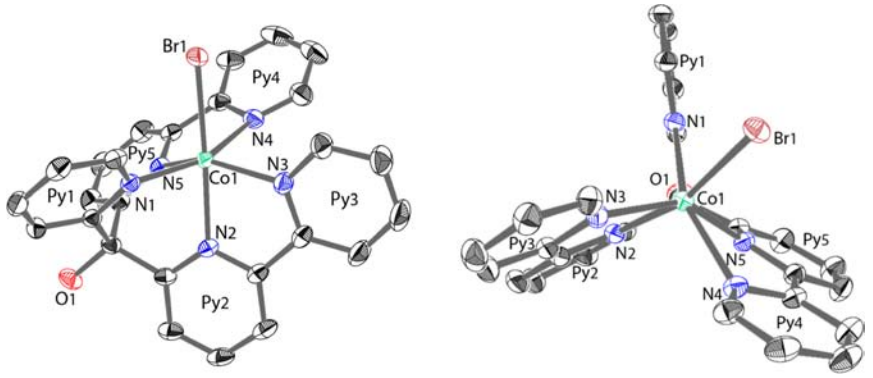

Figure 3. Left: ORTEP drawing of **2c**. Right: ORTEP drawing of **2c** along the Co_1–O_1 axis, both at 50% probability level with labeled nitrogen atoms and pyridine rings. Counterions, solvent molecules, and hydrogen atoms are omitted for clarity.

Table 2. Selected Bond Angles [deg] and Lengths [Å] of Complexes [MBr(2)]Br

	2a	2b	2c	2d	2f	2f
N_2–M–N_4 (α_{21})	115.66(6)	110.26(8)	111.74(7)	110.09(12)	109.04(6)	110.76(12)
N_2–M–N_5 (α_{22})	79.66(6)	79.01(8)	82.93(7)	85.45(13)	85.28(6)	82.00(13)
N_2–M–N_3 (α_{23})	72.54(6)	74.05(8)	75.60(7)	77.92(13)	80.30(7)	74.91(15)
N_2–M–N_1 (α_{24})	76.96(6)	77.99(8)	78.47(7)	79.80(12)	83.97(7)	75.00(13)
N_1–M–N_3 (β_{21})	121.60(6)	117.10(9)	113.06(7)	107.08(13)	131.54(7)	119.41(13)
N_3–M–N_4 (β_{22})	92.44(6)	88.19(9)	89.36(7)	91.51(13)	81.05(6)	88.04(14)
N_4–M–N_5 (β_{23})	71.01(6)	72.71(9)	73.60(7)	76.06(13)	66.55(6)	72.25(14)
N_5–M–N_1 (β_{24})	81.26(6)	86.06(9)	88.31(7)	88.59(13)	85.43(6)	84.44(13)
N_2–M–Br_3 (γ_{21})	156.27(4)	161.30(6)	165.51(5)	167.41(9)	170.92(5)	163.32(9)
Py_4–N_4–M (δ_{21})	161.74(10)	157.88(16)	156.51(10)	157.90(16)	141.50(11)	147.8(2)
Py_4–N_3–M (δ_{22})	173.31(10)	166.10(17)	172.93(11)	167.15(18)	172.12(12)	161.1(2)
M–N_4	2.2587(16)	2.278(3)	2.272(2)	2.184(3)	2.8113(17)	2.381(5)
M–$N_{1-3,5}$ (av)	2.27	2.19	2.13	2.07	2.09	2.17

dx.doi.org/10.1021/ic4004017 | Inorg. Chem. 2013, 52, 6055−6061

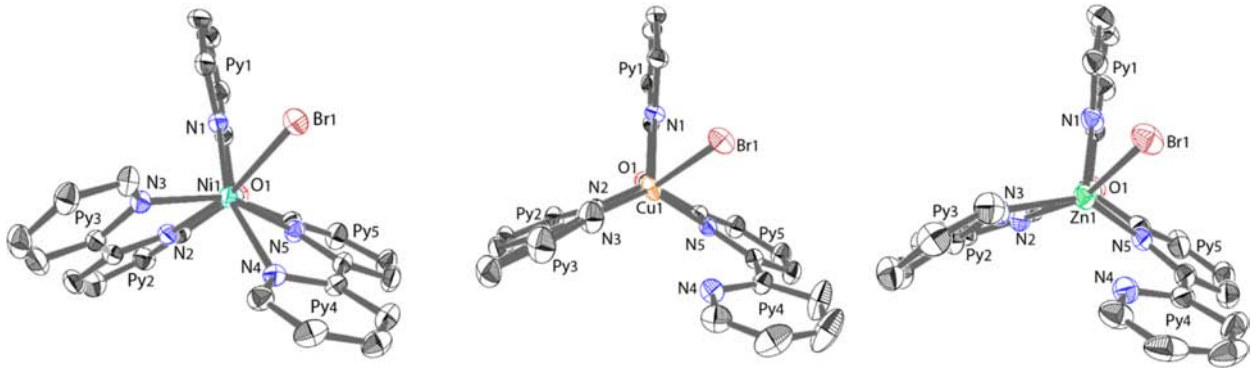

Figure 4. ORTEP drawings of **2d** (left), **2e** (middle), and **2f** (right) along the M_1-O_1 axis at 50% probability level with labeled nitrogen atoms and pyridine rings. The counterions, solvent molecules, and hydrogen atoms are omitted for clarity.

representations of the complexes and important crystallographic data are given in the Supporting Information (Tables S1 and S2).

In contrast to **1**, the geometry of ligand **2** does not offer a regular coordination pocket. Whereas coordination with **1** leads exclusively to six-membered chelate rings, the 2,2′-bipyridine ligands in **2** impose two five-membered rings, leading to sterical constraints and, hence, to strongly distorted octahedral structures for complexes **2a**–**f** (Figure 3 for **2c**, SI for other complexes).

One pyridine nitrogen atom (N_2) of one of the bipyridine subunits and one bromide occupy the axial positions in the coordination polyhedron. For all complexes, the N_2-M-Br_1 angles (γ_{21}) are significantly deflected from 180° (by 19.1–34.3°, Table 2). The remaining four pyridine nitrogen atoms occupy the equatorial positions. They do not form a plane as in **1a**–**f**, but the bond angles $N_{ax}-M-N_{eq}$ ($\alpha_{21}-\alpha_{24}$) as well as the equatorial N–M–N angles ($\beta_{21}-\beta_{24}$) strongly deviate from 90 °C (by −17.5 to +21.7 and −21.5 to +41.5°, respectively, Table 2). Due to these strong distortions from octahedral coordination geometry, complexes **2a**–**f** could also be described as showing distorted trigonal prismatic geometry. Figure 3 also shows the crystal structure of **2c** along the Co_1-O_1 axis, which corresponds to the C_3 rotation axis in an ideal trigonal prism. In this case, N_1, N_2, and N_5 form one and N_3, N_4, and Br_1 the other triangular face. While the first face is equilateral, the second one is not. Both faces are though more twisted toward an antiprism or octahedron, respectively. It is obvious from Figure 3 that the two bipyridine subunits do not coordinate in an optimal bidentate fashion, which is indicated by the angle between the pyridine rings ($Py_{2,3}$) and the corresponding $M-N_{3,4}$ bond (δ_{21} and δ_{22}, Table 2). Complexes with late 3d elements such as Cu^{2+} or Zn^{2+} show this distinct distortion (Figure 4). Although Py_4 in **2c** is turned with respect to the bipy plane, $Co-N_4$ interaction can still be described as binding (bond length = 2.272(2) Å). For the Cu^{2+} and Zn^{2+} complexes, however, the deviation of Py_4 from the plane (deviation from linearity: 38° for Cu, and 33° for Zn, Table 2) and the $M-N_4$ distance (2.8113(17) for Cu and 2.381(5) for Zn, respectively) are in comparison to the averaged $M-N_{1-3,5}$ bond lengths (2.09 for Cu and 2.17 for Zn, respectively) too far away. Thus, at least one pyridine is not bound in **2e** and **2f**, and these complexes are 5-fold rather than 6-fold coordinated. When designing ligand type **2**, we aimed at complexes that are stable in water due to their multidentate coordination and despite their distorted geometries. Following nature's model of the entatic state, such complexes may show enhanced reactivity as compared to systems with perfect ligand environment.[29] Ligand **2** possesses these properties as evidence from the X-ray structures shows. In line with this approach are recently prepared 3d element complexes with a hexadentate, tris-bipyridine based ligand. These complexes show rather trigonal prismatic than octahedral coordination but have not been studied with respect to their reactivities.[32]

Cyclovoltammetry (CV) provides relevant data for assessing relative catalytic activities of WRCs.[7] Electrochemical data for **1c** and **2c** were received from cyclovoltammetry and differential pulse polarography (DPM) at 1 mM concentrations in water (0.1 M $NaBF_4$) by means of a glassy carbon electrode. Complex **1c** exhibited a reduction potential (Co^{II}/Co^{I}) at the edge of the solvent window. A cyclic voltammogram could not be obtained in water. DPM showed a reduction potential $Co^{II/I}$ at −1.3 V (vs Ag/AgCl). In contrast, $E^{\circ}_{1/2}$ for **2c** was found at −0.87 V (Figure 5) and WRC **4** at −1.11, respectively[24] (vs Ag/AgCl), attributable to a $Co^{II/I}$ redox process. If this trend toward less negative potentials is a consequence of the distorted structure or the number of bipyridines in the ligand framework remains to be clarified. A characteristic catalytic wave for water reduction (S19) was observed in CV with **2c** under acidic conditions. Other cobalt polypyridine species such as the

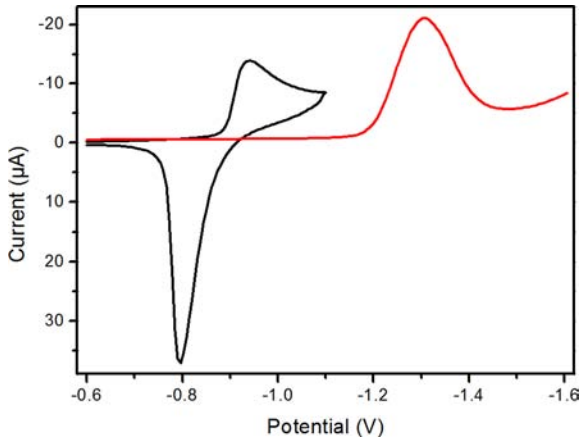

Figure 5. Cyclic voltammogram of 1 mM **2c** (black line) and differential pulse polarogram of 1 mM **1c** (red line) in 0.1 M $NaBF_4$ versus Ag/AgCl. The strong peak in the oxidation wave indicates reoxidation of precipitated **2c**, formed upon reduction onto the electrode surface. Repeated sweeps did not change the shape of the two waves, which indicates that **2c** is not decomposed during this process.

dx.doi.org/10.1021/ic4004017 | Inorg. Chem. 2013, 52, 6055–6061

original $[Co^{II}(bpy)_3]^{2+}$ and a recently reported complex with a pentadentate ligand consisting of one bipyridine, two pyridines, and a tertiary amine, showed $Co^{II/I}$ reduction potentials of −1.42 and −1.12 V (Ag/AgCl) in aqueous solution.[23,33] The aforementioned cobalt complex with a hexadendate tris-(bipyridine)methanol ligand exhibited a reduction potential of −1.18 V (Fc/Fc^+) in acetonitrile.[32]

H_2 formation studies in water with **1c** and **2c** were performed in order to evaluate ligand influence on photocatalytic activity. Photocatalytic water reduction was performed in water with 1 M ascorbic acid/sodium ascorbate buffer ($[H_2asc]/[Hasc]^-$ = 1:1, pH = 4.1), 0.5 mM PS **3**, and 5 μM WRC (385 nm LED). Both, **1c** and **2c**, produced H_2 under light irradiation (Figure 6). None of the complexes **1a**, **1b**, **1d**−**e**, and **2a**, **2b**, **2d**−**e**,

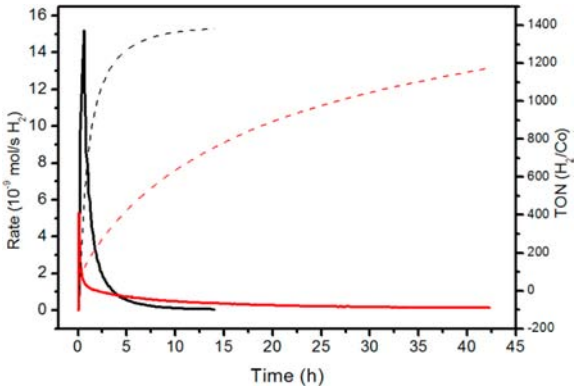

Figure 6. Rate profiles (bold lines: red, **1c**; black, **2c**) and TONs (dashed lines: red, **1c**; black, **2c**) in 10 mL of H_2O, 1 M $H_2asc/[Hasc]^-$ (pH 4.1), 0.5 mM **3**, and 5 μM Co-catalyst.

respectively, showed any photocatalytic activity. We had expected some activity with **1e** or **2e** since Ni^{2+} in general and congeners of Co^{2+} complexes in particular efficiently reduce water.[13,34] As shown in Figure 6, both catalysts **1c** and **2c** are active and reached similar TONs, 1180 H_2/Co for **1c** and 1380 for **2c**, respectively. This corresponds to a total amount of approximately 1.5 and 1.7 mL of hydrogen (59 μmol and 69 μmol, respectively). H_2 is formed at a faster rate for **2c** (distorted geometry) than for **1c** (regular structure). WRC **2c** produced about the same amount of H_2 in 5−10 h as compared to 45 h for **1c**. The fast decline in rate of hydrogen evolution is due to self-inhibition (short cut) of the catalytic system by dehydroascorbic acid, as previously reported.[25]

A WRC concentration dependency study (25, 15, 5, 0.5, and 0.1 μM, respectively, Figure 7) corroborates the enhanced activity of **2c** over **1c**. Both complexes achieved similar TONs in the concentration range 5−25 μM, but **2c** developed a 2−3 times higher maximal turnover frequency TOF_{max} (mol H_2) (mol Co^{-1}) (h^{-1}). Lowering the WRC concentration to 0.5 and 0.1 μM, TONs for **2c** increased substantially (up to 10 800), whereas activity for **1c** was lost. The smooth increase of the maximal TOF between 5 and 25 μM indicates light limitation of the process. Complex **2c** displayed a maximal TOF of 920 (5 μM) and 230 (mol H_2) (mol Co^{-1}) (h^{-1}) (25 μM), respectively. Consequently, approximately the same amount of H_2/WRC was produced in the range of the maximal TOF under both conditions. The absolute amounts of H_2 followed about the linearly of one of the TOFs. Below 0.5 μM, the dependencies change and the process is likely to become WRC

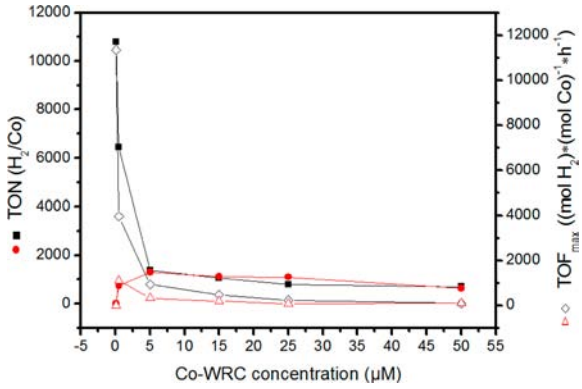

Figure 7. Cobalt dependency study with TONs in Co (filled symbols: red, **1c**; black, **2c**) and TOF_{max} (edged symbols: triangle, **1c**; diamond, **2c**) in 10 mL of H_2O, 1 M $H_2asc/[Hasc]^-$ (pH 4.1), 0.5 mM PS **3**. The maximal turnover frequency was maintained during around 10−20 min.

limited since TOFs and TONs strongly increase for **2c** (Figure 7).

The light path through the reaction solution is approximately 3 cm, but at 0.5 mM in PS **3**, 99% of the light is absorbed within 2 cm (2126 M^{-1} cm^{-1} at 385 nm, Figure S17). To achieve light absorption throughout the flask, the PS concentration was reduced to 0.25 mM. Catalysis with 0.25 mM **3** and 0.1 μM **2c** retained TON in Co of 10 400, but lead to a significant increased TOF_{max} as compared to 0.5 mM in PS **3** (Figure 8). At 0.25 mM, incident light is more uniformly absorbed; therefore, the concentration of effectively active cobalt catalyst and, thus, the hydrogen evolution must be higher.

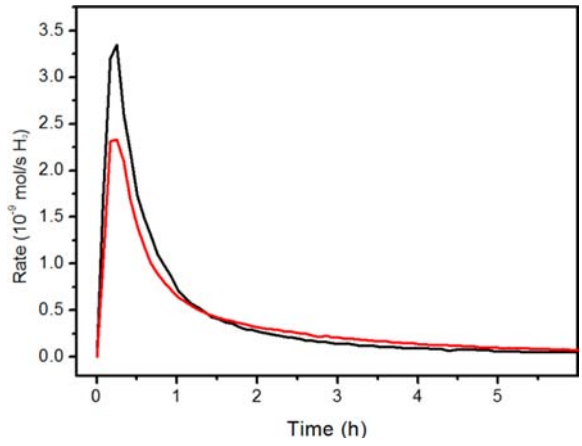

Figure 8. Photosensitizer concentration dependency: rate profile of photocatalysis in 10 mL H_2O, 1 M $H_2asc/[Hasc]^-$ (pH 4.1), 0.1 μM **2c**, and 0.5 mM (red line) and 0.25 mM **3** (black line), respectively.

Blank experiments with 1 M $H_2asc/[Hasc]^-$ buffer at pH = 4.1 and 0.5 mM PS **3** but without WRCs **1c** or **2c** yielded about one turnover in rhenium (H/Re) with complete decomposition of **3** as evident from HPLC before and after "catalysis". In the presence of WRC **2c**, PS **3** persisted after catalysis and no decomposition was observed (Figures S1 and S2). Thus, the released H_2 can be accounted quantitatively to the catalytic cycle rather than to decomposition of **3**. To exclude cobalt colloids as the catalytically active species, a Hg poisoning experiment was performed as reported for other systems.[20,35]

dx.doi.org/10.1021/ic4004017 | Inorg. Chem. 2013, 52, 6055−6061

Catalysis with 1 M ascorbate buffer, 0.5 mM **3**, and 5 μM **2c**, and 1.4 g mercury resulted in a very similar rate profile; thus, **2c** is assumed to be the active catalyst (see Figure S32).

CONCLUSION

To extend the polypyridyl ligand platform, we synthesized the pentadentate bis-2,2′-bipyridine-pyridine based ligand **2** and a selected series of its complexes with dicationic first row transition elements. Structural analyses provided evidence that this ligand does not offer a cavity ideal for octahedral coordination geometry. On the contrary, complex structures are strongly distorted from octahedral to a trigonal prismatic. Whereas such structural distortions lead to less stable complexes, they often display increased reactivity. Accordingly, under light irradiation, **2c** (Co^{II}) showed significant improvement on water reduction activity as compared to **1c**, whose pentadentate, pyridine-based ligand **1** coordinates to Co^{II} in an almost ideal octahedral geometry. The study of ligand systems with similar electronic but different geometrical properties will lead to a better understanding of how ligand frameworks influence the activity of water reducing catalysts.

EXPERIMENTAL SECTION

Instrumentation. Details are given in the Supporting Information.

Syntheses. 6-Bromo-2,2′-bipyridine (**5**) was synthesized on a 100 g scale according to a previously published procedure,[36] but an alternative method for purification was developed. The intermediate 1-methyl-6-(2-pyridyl)pyridine-2(*H*)-one was purified by recrystallization from EtOAc/iPr_2O. The product 6-bromo-2,2′-bipyridine (**5**, Br-bpy) was purified by filtration through silica (EtOAc/hexane 9:1) followed by recrystallization from hexane. [Re(py)(bpy)$(CO)_3$]OTf and 2,2′-bipyridin-5-yl(2,2′-bipyridin-6-yl)pyridin-2-ylmethanol (**1**) were synthesized according to literature procedures.[37,26]

2,2′-Bipyridin-6-yl(pyridin-2-yl)methanone (6). The synthesis was adapted from a reported procedure.[38] A solution of 6-bromo-2,2′-bipyridine (680 mg, 2.89 mmol) in dry diethyl ether (15 mL) was cooled to −78 °C, and n-butyllithium 1.6 M (1.989 mL, 3.18 mmol) was added dropwise. The deep red solution was stirred for 1 h. Then, a solution of ethyl picolinate (0.430 mL, 3.18 mmol) in dry THF (10 mL) was added dropwise. The mixture was allowed to warm up to −40 °C, stirred for 1 h at this temperature, quenched with MeOH, and allowed to come to room temperature (rt). CH_2Cl_2 and HCl (2 M) were added and the phases separated. The organic phase was extracted three times with 2 M HCl. The combined aqueous phases were neutralized with NaOH (2 M), and extracted three times with CH_2Cl_2. The combined organic phases were dried over $MgSO_4$, filtered, and concentrated to dark red oil. The crude mixture was purified by flash chromatography (40g C18 silica, H_2O/MeOH = 9:1 to 0:1 within 1 h, 20 mL/min, crude put on the column adsorbed on celite) to obtain 2 fractions with the desired product (70%). Analysis is correct and in agreement with literature.

Di-2,2′-bipyridin-6-yl(pyridin-2-yl)methanol (2). n-BuLi (1.6 M, 1.0 mL, 1.60 mmol) was added dropwise to a solution of Br-bpy (**5**) (376 mg, 1.60 mmol) in dry Et_2O (20 mL) at −78 °C (dark red solution). After 1 h, 2,2′-bipyridin-6-yl(pyridin-2-yl)methanone (380 mg, 1.454 mmol) was added in small portions and the dark greenish solution stirred for 1h. The reaction mixture was quenched with MeOH (color change to red) and allowed to come to rt. HCl (2 M) and CH_2Cl_2 were added and the phases separated. The organic phase was extracted three times with HCl (2 M), the combined water phases were neutralized with NaOH (2 M) and extracted three times with CH_2Cl_2. The combined organic phases were dried over $MgSO_4$, filtered, and concentrated to a dark red-brown oil. The crude mixture was purified by flash chromatography (40g C_{18}-silica, H_2O/MeOH = 9:1 to 0:1 within 1.25 h, 20 mL/min, crude adsorbed on celite) to obtain the desired ligand as a slightly brownish solid (40%). Impure fractions were further purified by digestion in iPr_2O.

^{1}H NMR (DMSO, 300 MHz): δ 7.23 (s, 1H), 7.34 (ddd, J_1 = 7.2 Hz, J_2 = 5.1 Hz, J_3 = 1.5 Hz, 1H), 7.40 (ddd, J_1 = 7.5 Hz, J_2 = 4.8 Hz, J_3 = 1.2 Hz, 2H), 7.73 (dd, J_1 = 7.8 Hz, J_2 = 1 Hz, 2H), 7.76−7.87 (m, 4H), 7.96 (t, J = 7.8 Hz, 2H) 8.17 (d, J = 8.1 Hz, 2H), 8.29 (dd, J_1 = 7.8 Hz, J_2 = 0.6 Hz, 2H), 8.52 (dm, J = 4.8 Hz, 1H), 8.65 (dm, J = 4.8 Hz, 2H), MS (ESI); m/z: 418 (98%, $[M + H]^+$), 440 (100%, $[M + Na]^+$), 456 (10%, $[M + K]^+$). Anal. Calcd for $C_{27}H_{19}N_5O$ (%): C, 74.80; H, 4.59; N, 16.78. Found: C, 74.49; H, 4.55, N, 16.41

General Procedure for Syntheses of Complexes 1a−f and 2a−f. Equimolar amounts of ligand and the corresponding MBr_2 salts were stirred in methanol at rt for 1−12 h (complete conversion checked by HPLC). The colored solutions were filtered through celite and concentrated. Purification was achieved by crystallization with the vapor diffusion method as outlined below. If not otherwise noted, single crystals suitable for X-ray analysis were obtained by the same method.[39] For electronic spectra of complexes **1a−f** and **2a−f**, respectively, see Figures S2−S14 and Figures S15 and S17.

[MnBr(PPy)]Br (1a). Slightly yellowish, vapor diffusion (MeOH/Et_2O). Anal. Calcd for [MnBr(PPy)]Br·Et_2O (%): C, 50.56; H, 4.24; N, 9.51. Found: C, 50.59; H, 4.03; N, 9.20. ESI-MS: m/z = 583 (100%, $[M - Br]^+$), 501 (20%, $[M - Br - H]^+$).

[MnBr(aPPy)]Br (2a). Slightly yellowish, vapor diffusion (MeOH/THF). Anal. Calcd for [MnBr(aPPy)]Br (%): C, 49.39; H, 3.03; N, 10.08. Found: C, 49.11; H, 3.21; N, 11.00. ESI-MS: m/z = 553 (100%, $[M - Br]^+$), 585 (20%, $[M - Br + MeOH]^+$).

[FeBr(PPy)]Br (1b). Yellow, vapor diffusion (MeOH/Et_2O). Single crystals obtained by layering Et_2O over a MeOH solution. Anal. Calcd for [FeBr(PPy)]Br·H_2O (%): C, 47.61; H, 3.40; N, 10.28. Found: C, 47.62; H, 3.48; N, 10.34. ESI-MS: m/z = 502 (100%, $[M - 2Br - H]^+$), 562 (80%, $[M - 2Br, PrO^-]^+$), 582 (70%, $[M - Br]^+$).

[FeBr(aPPy)]Br (2b). Dark red, vapor diffusion (MeOH/THF). Anal. Calcd for [FeBr(aPPy)]Br·Et_2O (%): C, 49.32; H, 3.02; N, 11.06. Found: C, 49.28; H, 3.04; N, 11.01, ESI-MS: m/z = 518 (100%, $[M - 2Br, + EtO]^+$), 552 (25%, $[M - Br]^+$).

[CoBr(PPy)]Br (1c). Rose, vapor diffusion (MeOH/Et_2O). Single crystals obtained by layering Et_2O over a MeOH solution. Anal. Calcd for [CoBr(PPy)]Br (%): C, 48.68; H, 3.18, N, 10.51. Found: C, 48.21; H, 3.17; N, 10.10. ESI-MS: m/z = 587 (100%, $[M - Br]^+$), 505 (80%, $[M - 2Br - H]^+$), 551 (55%, $[M - 2Br + EtO]^+$).

[CoBr(aPPy)]Br (2c). Brown, vapor diffusion (MeOH/Et_2O). Anal. Calcd for [CoBr(PPy)]Br·H_2O (%): C, 48.18; H, 3.16; N, 10.80. Found: C, 48.26; H, 3.20; N, 11.32. ESI-MS: m/z = 557 (100%, $[M - Br, - H]^+$, 475 (70%, $[M - 2Br, - H]^+$, 507 (40%, $[M - 2Br + MeO]^+$.

[NiBr(PPy)]Br (1d). Light purple, vapor diffusion (MeOH/THF). Anal. Calcd for [NiBr(PPy)]Br (%): C, 48.69; H, 3.18;

dx.doi.org/10.1021/ic4004017 | Inorg. Chem. 2013, 52, 6055−6061

N, 10.52. Found: C, 48.34; H, 3.15, N, 10.25. ESI-MS: m/z = 586 (100%, $[M - Br]^+$), 618 (60%, $[M - Br + MeOH]^+$).

[NiBr(aPPy)]Br (2d). Brown, vapor diffusion (MeOH/hexane). Anal. Calcd for [NiBr(aPPy)]Br (%): C, 49.10; H, 3.01; N, 11.01. Found: C, 49.12; H, 3.20; N, 10.81. ESI-MS: m/z = 556 (100%, $[M - Br]^+$).

[CuBr(PPy)]Br (1e). Blue, vapor diffusion (MeOH/THF). Anal. Calcd for $[CuBr(PPy)]Br\cdot{}^1/_2THF$ (%): C, 49.27; H, 3.56; N, 9.91. Found: C, 49.31; H, 3.45; N, 9.49. ESI-MS: m/z = 591 (100%, $[M - Br]^+$).

[CuBr(aPPy)]Br (2e). Blue, vapor diffusion (MeOH/THF). Anal. Calcd for [CuBr(aPPy)]Br (%): C, 48.73; H, 2.99; N, 10.93. Found: C, 49.09; H, 3.24; N, 10.46. ESI-MS: m/z = 561 (100%, $[M - Br]^+$), 480 (40%, $[2\ M - Br - H]^{2+}$.

[ZnBr(PPy)]Br (1f). Colorless, vapor diffusion (MeOH/Et_2O). Anal. Calcd for $[ZnBr(PPy)]Br\cdot H_2O$ (%): C, 46.95; H, 3.36; N, 10.14. Found: C, 46.83; H, 3.43; N, 9.99. ESI-MS: m/z = 592 (100%, $[M - Br]^+$). ^{1}H NMR (300 MHz, DMSO): δ 7.6−7.75 (m, 4H), 8.1−8.3 (m, 13H), 8.5−8.6 (m, 2H).

[Zn(aPPy)Br_2] (2f). Colorless, vapor diffusion, (MeOH/Et_2O). Anal. Calcd for $[ZnBr(aPPy)]Br\cdot{}^1/_2H_2O$ (%): C, 47.92; H, 3.09; N, 10.75. Found: C, 47.86; H, 3.06; N, 10.56. ESI-MS: m/z = 562 (100%, $[M - Br]^+$). ^{1}H NMR (300 MHz, DMSO): δ 7.55 (t, J = 6.9 Hz, 1H), 7.89 (t, J = 6.6 Hz, 2H), 8.05−8.18 (m, 2H), 8.3−8.5 (m, 6H), 8.6−8.8 (m, 6H), 9.21 (d, J = 4.5 Hz).

■ ASSOCIATED CONTENT

Ⓢ Supporting Information

Crystallographic data in CIF format, electronic spectra of complexes, HPLC traces, experimental photocatalytic conditions. This material is available free of charge via the Internet at http://pubs.acs.org

■ AUTHOR INFORMATION

Corresponding Author

*E-mail: ariel@aci.uzh.ch.

Notes

The authors declare no competing financial interest.

■ ACKNOWLEDGMENTS

We thank the Swiss National Science Foundation, Sinergia Project CRSII2-136205/1, for financially supporting this project.

■ REFERENCES

(1) Blankenship, R. E.; Tiede, D. M.; Barber, J.; Brudvig, G. W.; Fleming, G.; Ghirardi, M.; Gunner, M. R.; Junge, W.; Kramer, D. M.; Melis, A.; Moore, T. A.; Moser, C. C.; Nocera, D. G.; Nozik, A. J.; Ort, D. R.; Parson, W. W.; Prince, R. C.; Sayre, R. T. *Science* **2011**, *332*, 805−809.

(2) Lewis, N. S.; Nocera, D. G. *Proc. Natl. Acad. Sci. U.S.A.* **2006**, *103*, 15729−15735.

(3) Balzani, V.; Credi, A.; Venturi, M. *ChemSusChem* **2008**, *1*, 26−58.

(4) Chu, S.; Majumdar, A. *Nature* **2012**, *488*, 294−303.

(5) Swiegers, G. F.; MacFarlane, D. R.; Officer, D. L.; Ballantyne, A.; Boskovic, D.; Chen, J.; Dismukes, G. C.; Gardner, G. P.; Hocking, R. K.; Smith, P. F.; Spiccia, L.; Wagner, P.; Wallace, G. G.; Winther-Jensen, B.; Winther-Jensen, O. *Aust. J. Chem.* **2012**, *65*, 577−582.

(6) Cook, T. R.; Dogutan, D. K.; Reece, S. Y.; Surendranath, Y.; Teets, T. S.; Nocera, D. G. *Chem. Rev.* **2010**, *110*, 6474−6502.

(7) Losse, S.; Vos, J. G.; Rau, S. *Coord. Chem. Rev.* **2010**, *254*, 2492−2504.

(8) Dempsey, J. L.; Brunschwig, B. S.; Winkler, J. R.; Gray, H. B. *Acc. Chem. Res.* **2009**, *42*, 1995−2004.

(9) Artero, V.; Chavarot-Kerlidou, M.; Fontecave, M. *Angew. Chem., Int. Ed.* **2011**, *50*, 7238−7266.

(10) Marinescu, S. C.; Winkler, J. R.; Gray, H. B. *Proc. Natl. Acad. Sci. U.S.A.* **2012**, *109*, 15127−15131.

(11) Eckenhoff, W. T.; Eisenberg, R. *Dalton Trans.* **2012**, *41*, 13004−13021.

(12) Gloaguen, F.; Rauchfuss, T. B. *Chem. Soc. Rev.* **2009**, *38*, 100−108.

(13) Jacques, P. A.; Artero, V.; Pecaut, J.; Fontecave, M. *Proc. Natl. Acad. Sci. U.S.A.* **2009**, *106*, 20627−20632.

(14) Karunadasa, H. I.; Chang, C. J.; Long, J. R. *Nature* **2010**, *464*, 1329−1333.

(15) Han, Z. J.; Qiu, F.; Eisenberg, R.; Holland, P. L.; Krauss, T. D. *Science* **2012**, *338*, 1321−1324.

(16) Kaes, C.; Katz, A.; Hosseini, M. W. *Chem. Rev.* **2000**, *100*, 3553−3590.

(17) Fihri, A.; Artero, V.; Pereira, A.; Fontecave, M. *Dalton Trans.* **2008**, 5567−5569.

(18) Lazarides, T.; McCormick, T.; Du, P. W.; Luo, G. G.; Lindley, B.; Eisenberg, R. *J. Am. Chem. Soc.* **2009**, *131*, 9192−9194.

(19) Hu, X.; Brunschwig, B. S.; Peters, J. C. *J. Am. Chem. Soc.* **2007**, *129*, 8988−8998.

(20) Du, P.; Schneider, J.; Luo, G.; Brennessel, W. W.; Eisenberg, R. *Inorg. Chem.* **2009**, *48*, 4952−4962.

(21) Bigi, J. P.; Hanna, T. E.; Harman, W. H.; Chang, A.; Chang, C. J. *Chem. Commun.* **2010**, *46*, 958−960.

(22) Sun, Y. J.; Bigi, J. P.; Piro, N. A.; Tang, M. L.; Long, J. R.; Chang, C. J. *J. Am. Chem. Soc.* **2011**, *133*, 9212−9215.

(23) Singh, W. M.; Baine, T.; Kudo, S.; Tian, S.; Ma, X. A. N.; Zhou, H.; DeYonker, N. J.; Pham, T. C.; Bollinger, J. C.; Baker, D. L.; Yan, B.; Webster, C. E.; Zhao, X. *Angew. Chem., Int. Ed.* **2012**, *51*, 5941−5944.

(24) Guttentag, M.; Rodenberg, A.; Bachmann, C.; Senn, A.; Hamm, P.; Alberto, R. *Dalton Trans.* **2013**, *42*, 334−337.

(25) Guttentag, M.; Rodenberg, A.; Kopelent, R.; Probst, B.; Buchwalder, C.; Brandstätter, M.; Hamm, P.; Alberto, R. *Eur. J. Inorg. Chem.* **2012**, *2012*, 59−64.

(26) Goldsmith, C. R.; Stack, T. D. P. *Inorg. Chem.* **2006**, *45*, 6048−6055.

(27) Goldsmith, C. R.; Cole, A. P.; Stack, T. D. P. *J. Am. Chem. Soc.* **2005**, *127*, 9904−9912.

(28) Grohmann, A. *Dalton Trans* **2010**, *39*, 1432−1440.

(29) McNaught, A. D.; Wilkinson, A. *IUPAC. Compendium of Chemical Terminology*, 2nd ed.; Blackwell Science: Oxford, U.K., 1997.

(30) Klein Gebbink, R. J. M.; Jonas, R. T.; Goldsmith, C. R.; Stack, T. D. P. *Inorg. Chem.* **2002**, *41*, 4633−4641.

(31) Lopez, J. P.; Heinemann, F. W.; Prakash, R.; Hess, B. A.; Horner, O.; Jeandey, C.; Oddou, J.-L.; Latour, J.-M.; Grohmann, A. *Chem.—Eur. J.* **2002**, *8*, 5709−5722.

(32) Knight, J. C.; Alvarez, S.; Amoroso, A. J.; Edwards, P. G.; Singh, N. *Dalton Trans* **2010**, *39*, 3870−3883.

(33) Pospisil, L.; Kuta, J. *J. Electroanal. Chem.* **1979**, *101*, 391−398.

(34) Collin, J.-P.; Jouaiti, A.; Sauvage, J.-P. *Inorg. Chem.* **1988**, *27*, 1986−1990.

(35) Cline, E. D.; Adamson, S. E.; Bernhard, S. *Inorg. Chem.* **2008**, *47*, 10378−10388.

(36) Norrby, T.; Börje, A.; Zhang, L.; Akermark, B. *Acta Chem. Scand.* **1998**, *52*, 77−85.

(37) Probst, B.; Guttentag, M.; Rodenberg, A.; Hamm, P.; Alberto, R. *Inorg. Chem.* **2011**, *50*, 3404−3412.

(38) Wolpher, H.; Johansson, O.; Abrahamsson, M.; Kritikos, M.; Sun, L.; Åkermark, B. *Inorg. Chem. Commun.* **2004**, *7*, 337−340.

(39) Spingler, B.; Schnidrig, S.; Todorova, T.; Wild, F. *CrystEngComm* **2012**, *14*, 751−757.